Research Article

Nitrogen-doped black TiO_2 spheres with enhanced visible light photocatalytic performance

Haiyang Liu[1] · Hongmei Fan[1] · Rong Wu[1] · Lie Tian[1] · Xi Yang[1] · Yanfei Sun[1]

Abstract

N-doped black TiO_2 spheres (N_2–b-TiO_2) were prepared by solvothermal reaction and calcination under a nitrogen atmosphere. N-doping introduces new impurity levels above the TiO_2 valence band, enhancing the effective absorption of visible light. The presence of O_V and Ti^{3+} in the disordered outer layer inhibits electron–hole pair recombination, and the spherical structure provides many active sites. Those were confirmed by X-ray diffraction, Fourier transform IR, X-ray photoelectron spectroscopy and High-resolution transmission electron microscopy. UV–visible absorption indicates that the nitrogen-doped black TiO_2 samples has a reduced band gap and a strong visible light absorption, which is attributed to the doping of O_V, Ti^{3+} and N. The photocatalytic efficiency of the best sample (N_2–b-TiO_2) for potassium dichromate and rhodamine B was 96.2% and 99.5%, respectively. The superoxide radical ($\bullet O_2^-$) played a dominant role in photocatalysis by scavenging experiments. Thus, a photocatalytic mechanism with reduced band gap has been proposed. This study provides a simple and practical method for non-metallic doping to control the photocatalytic performance of semiconductors.

✉ Rong Wu, wurongxju@sina.com | [1]School of Physics Science and Technology, Xinjiang University, Urumqi 830000, Xinjiang, China.

SN Applied Sciences (2019) 1:487 | https://doi.org/10.1007/s42452-019-0502-8

Received: 25 January 2019 / Accepted: 17 April 2019 / Published online: 24 April 2019

Graphical Abstract

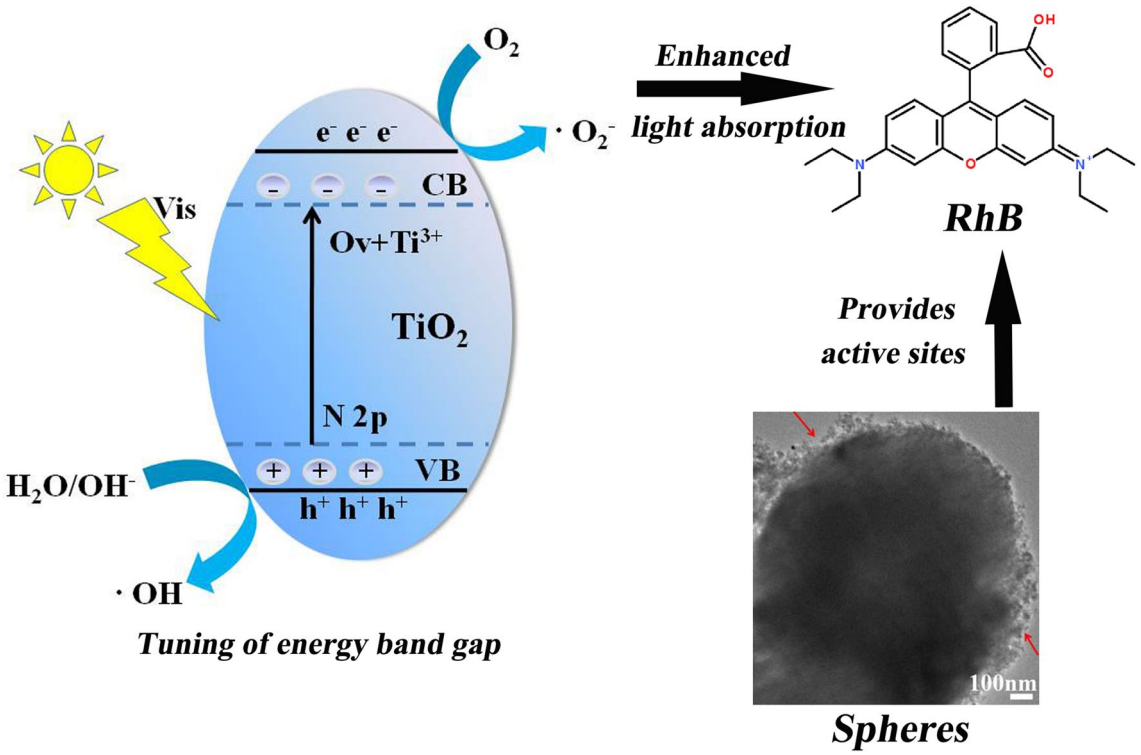

Keywords Nitrogen-doped · Black TiO_2 spheres · Photocatalytic degradation · Band structure

1 Introduction

Modification of the semiconductor photocatalyst can be achieved by doping, formation of heterojunctions, and changing the phase structure [1–4]. Doping has been used as a simple and easy method, in which non-metal doping has been proven to be a effective way to expand the photoresponse range of semiconductors [5, 6]. TiO_2 is a promising semiconductor catalyst for its low cost, excellent stability, and non-toxicity [7–9]. However, The absorption of visible light by TiO_2 is less than 5%, and its photogenerated electron–hole pairs are rapidly recombined, resulting in low photocatalytic activity. Many reports suggest that doping with nitrogen is a simple and effective method to improve the photocatalytic performance of TiO_2 [10]. The results of calculations show that, because of the mixing of the N 2*p* states with O 2*p* states in the valence bands, the substitutional doping of N for O reduces the bandgap and increases the visible-light photocatalytic activity [11]. Asahi et al. [12] prepared nitrogen-doped TiO_2 films by sputtering, and these films showed good photocatalytic activity in the visible light range. Although nitrogen doping can achieve visible light absorption from 400 to 600 nm, it is still difficult to achieve light absorption in a broader range (400–800 nm). In 2011, Chen et al. presented a black TiO_2 with a highly disordered surface layer and a visible light absorption range of 400–1200 nm [13]. At present, methods of preparing black TiO_2 include high-pressure hydrogenation, chemical reduction, and chemical oxidation [14–17]. However, the shortcomings of these methods include long reaction times, expensive chemicals, and complex operation.

Recently, more researchers have paid attention to the modification of the microstructure of black TiO_2 to improve its photocatalytic properties, such as the use of a spherical morphology. Black TiO_2 spheres have a high specific surface area, which provides many active reaction sites for photocatalytic activity [17–19]. Hu et al. [20] prepared a black TiO_2 hollow sphere with a relatively high surface area of 80 $m^2\ g^{-1}$ and a high photocatalytic hydrogen evolution rate (241 μmmol h^{-1} 0.1 g^{-1}), but the preparation method requires dangerous high-temperature hydrogenation. Although black N-TiO_{2-x} hollow spheres have a large specific surface area of 128 $m^2\ g^{-1}$ and show a high visible-light-driven photocatalytic degradation ratio for phenol (up to 95%), the degradation process is time-consuming

(210 min) [21]. Therefore, simpler and safer methods for preparing nitrogen-doped black TiO_2 spheres with excellent photocatalytic activity are urgently required.

Herein, we propose a solvothermal method combined with calcination under a nitrogen atmosphere to prepare black N-doped TiO_2 spheres to improve the photocatalytic performance. The relationship between the structure and the photocatalytic performances was also explored by comparing the behaviour of black TiO_2 spheres and N-doped black TiO_2 spheres. In addition, the photocatalytic mechanism of the N-doped black TiO_2 spheres is also proposed. This study will have widespread practical application in the environmental field.

2 Experimental

2.1 Materials

Titanium(IV) sulfate ($Ti(SO_4)_2$), dodecyltrimethylammonium bromide (CTAB), ammonium chloride (NH_4Cl), and hydrochloric acid (HCl) were purchased from Sinopharm Chemical Reagent Co., Ltd., (China) and used without further purification.

2.2 Synthesis of the N-doped black TiO_2 spheres

The N-doped black TiO_2 spheres were prepared via a solvothermal method, followed by calcination under a nitrogen atmosphere. In a typical process, titanium(IV) sulfate (0.5 g), dodecyltrimethylammonium bromide (0.1 g), and absolute ethanol (10 mL) were mixed together. Then, different amounts of ammonium chloride were dissolved in a mixture of hydrochloric acid (1 mL) and distilled water (20 mL). The second solution was gradually added to the first and then stirred for 2 h at room temperature, followed by transfer to an autoclave and heating at 180 °C for 12 h. Afterwards, the samples were gradually cooled to room temperature. The product was obtained from the autoclave by centrifuging thrice with deionised water and ethanol and drying at 60 °C for 3 h. Subsequently, the final products were transferred into porcelain boats and calcined at 500 °C for 3 h under an N_2 atmosphere. Cooling to room temperature yielded the nitrogen-doped black TiO_2 spheres. The samples of nitrogen-doped black TiO_2 spheres are denoted N_n–b-TiO_2, where *n* represents the mole ratio of ammonium chloride to TiO_2, i.e. 0:1, 1:1, 2:1, and 3:1. The final products are, thus, N_0–b-TiO_2, N_1–b-TiO_2, N_2–b-TiO_2, and N_3–b-TiO_2.

2.3 Material characterisation

The crystal structures and stabilities of the samples were characterised by X-ray diffraction (XRD) (Bruker D8 Advance). Transmission electron microscopy (TEM) (Tecnai G2 F20) was used to study the morphologies and atomic arrangement of the samples. The morphologies of the samples were characterised by scanning electron microscopy (SEM) (LEO1430VP). The chemical composition was investigated by energy dispersive spectroscopy (EDS) (LEO1430VP). Fourier transformation infrared (FT-IR) spectra were obtained on a Nicolet 500 spectrometer. X-ray photoelectron spectroscopy (XPS) (Thermo ESCALAB 250XI) was used to determine the surface electron states of the samples and the concentration of each phase in the mixed phases. The optical properties were characterised by PerkinElmer UV/Vis spectrometer (Lambda 650 S) at room temperature.

2.4 Photocatalytic measurements

The measurements of the photocatalytic activity were carried out at room temperature by the degradation of potassium dichromate (Cr(VI)) and rhodamine B (RhB) dyes. A 350-W Xe light equipped with an optical filter ($\kappa \geq 420$ nm) served as the source of simulated sunlight. In the photocatalytic test, 10 mg of the sample were placed in a 50-mL beaker with 40-mL aqueous suspensions of potassium dichromate (Cr(VI)) and RhB (20 mg L^{-1}), respectively. Before irradiation, the suspensions were magnetically stirred in the dark for 30 min to establish adsorption/desorption equilibrium between dyes and the photocatalyst. Circulating water was used to cool the solution and to prevent solvent evaporation. During the measurement process, 4-mL aliquots suspensions were collected at intervals (30 min) for analysis after centrifugation. The concentration of RhB was monitored by measuring the absorbance

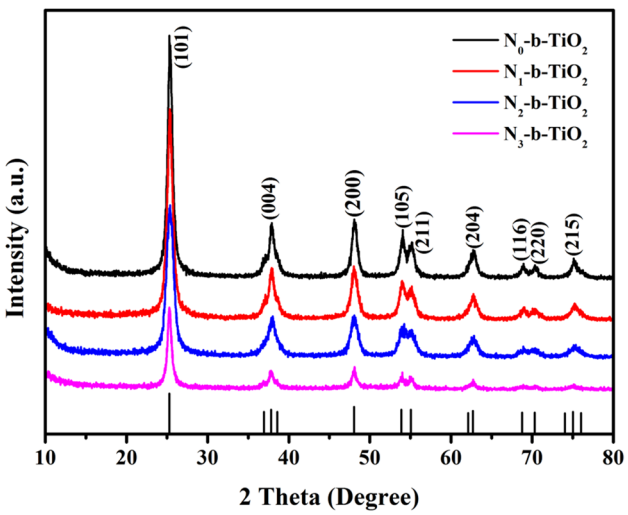

Fig. 1 XRD patterns of N_0–b-TiO_2, N_1–b-TiO_2, N_2–b-TiO_2, and N_3–b-TiO_2, respectively

Table 1 The 2θ values of observed reflections, their FWHM, and the crystallite sizes of different samples

Samples	Diffraction angle (°)	FWHM (rad)	Crystallite size (nm)
N_0–b-TiO_2	12.72	0.0136	10.33
N_1–b-TiO_2	12.70	0.0113	12.34
N_2–b-TiO_2	12.67	0.0101	12.88
N_3–b-TiO_2	12.68	0.0092	13.91

at 554 nm using a UV/Vis spectrometer (Lambda 650 s, Perkin Elmer, USA). The Cr(VI) concentration in the filtrate was measured using the standard 1,5-diphenylcarbazide colorimetric method by measuring the purple complex at 540 nm using the UV–VIS spectrophotometer [22].

3 Results and discussion

The crystal phases and crystallinity of N_0–b-TiO_2, N_1–b-TiO_2, N_2–b-TiO_2, and N_3–b-TiO_2 were studied by X-ray diffraction analysis, as shown in Fig. 1. All the samples show similar patterns that are consistent with the standard card of anatase TiO_2 (No. JCPDS 21-1272). A series of characteristic peaks at 2θ = 25.31°, 37.80°, 48.04°, 53.89°, 55.06°, 62.68°, 68.76°, 70.30°, and 75.02° were observed, and these correspond to the (101), (004), (200), (105), (211), (204), (116), (220), and (215) planes of anatase TiO_2, respectively [23, 24]. With increasing ammonium chloride, the anatase (101) peak of N-doped black TiO_2 spheres became broader and less intense [25]. Table 1 shows the 2θ values, full width half maximum (FWHM), and crystallite sizes of N_0–b-TiO_2, N_1–b-TiO_2, N_2–b-TiO_2, and N_3–b-TiO_2. As calculated from the most intense peak of the anatase phase (101), the grain sizes of N_0–b-TiO_2, N_1–b-TiO_2, N_2–b-TiO_2, and N_3–b-TiO_2 were found to be 10.33, 12.34, 12.88, and 13.91 nm, respectively. These results show that, as the content of ammonium chloride increases, the crystallite size of the sample gradually increases [26].

The composition and surface functional groups of the N_0–b-TiO_2, N_1–b-TiO_2, N_2–b-TiO_2, and N_3–b-TiO_2 samples were analysed by FT-IR (Fig. 2a). All samples show similar spectra, corresponding to the stretching of the hydroxyl groups at around 3448 cm^{-1}, and the peak at 1604 cm^{-1} arises from the stretching of the O–H bond. In comparison with N_0–b-TiO_2, the N_1–b-TiO_2, N_2–b-TiO_2, and N_3–b-TiO_2 samples display additional peaks at around 1426 and

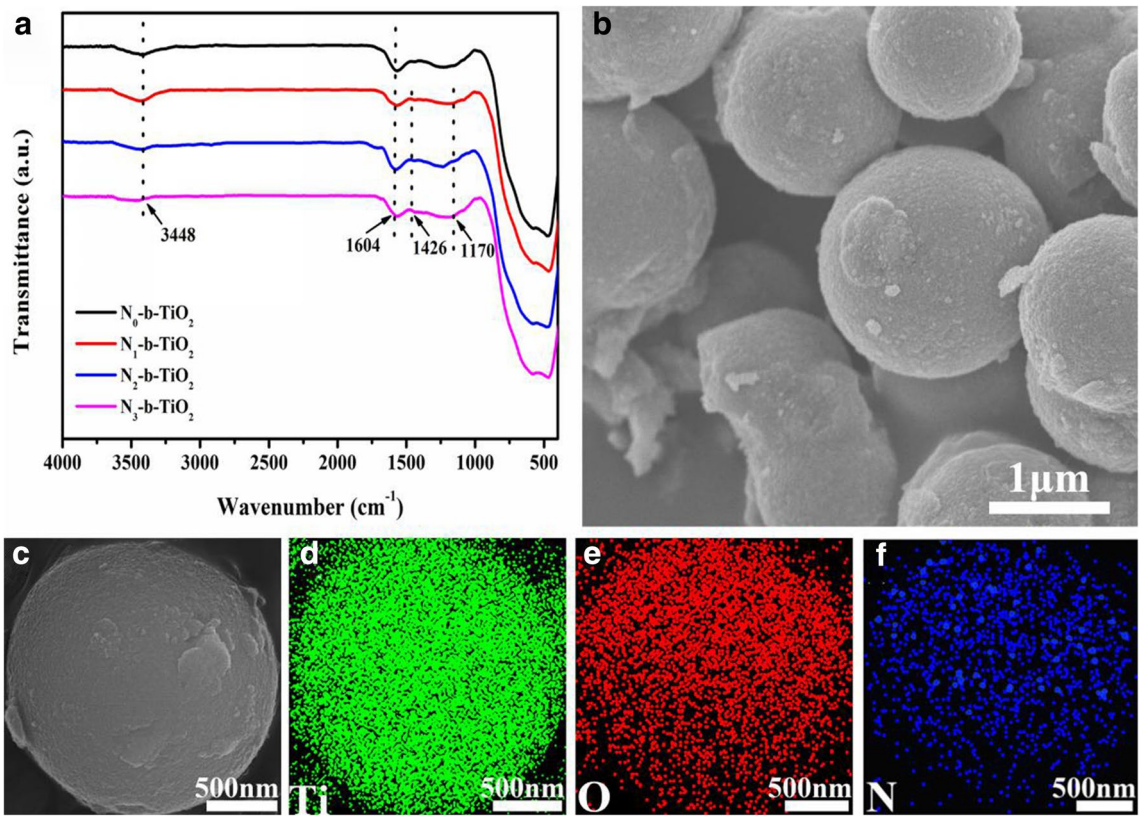

Fig. 2 **a** FT-IR spectra of N_0–b-TiO_2, N_1–b-TiO_2, N_2–b-TiO_2, and N_3–b-TiO_2. **b** SEM images of the N_2–b-TiO_2 spheres. **c**–**f** EDS mapping results of the N_2–b-TiO_2 spheres: **d** Ti, **e** O, and **f** N

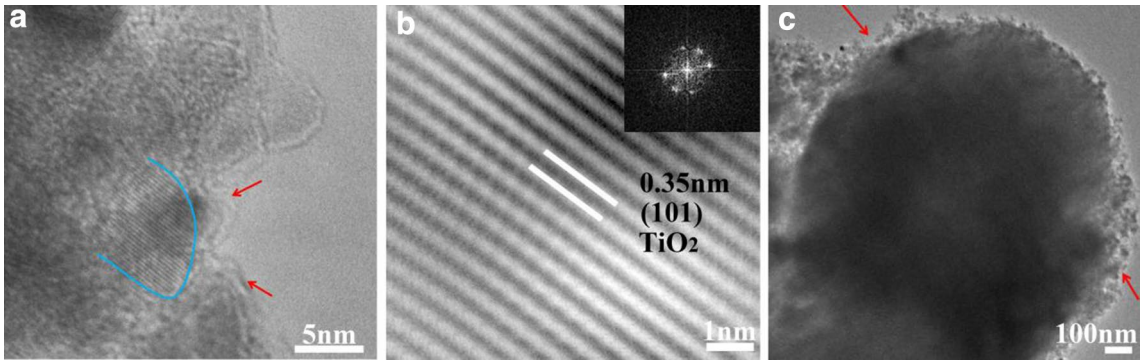

Fig. 3 **a** High-resolution HRTEM images of the N_2–b-TiO_2 sample. **b** HRTEM images of the region enclosed by the blue line in (**a**). Inset: Fast Fourier transform image of N_2–b-TiO_2. **c** Low-magnification TEM images of the N_2–b-TiO_2 sample

1170 cm^{-1}, which are attributed to the vibrations of the N-Ti bonds. The appearance of the N-Ti bond in the samples suggests that N had been successfully incorporated into the black TiO_2 lattice [27, 28]. The morphologies of the N_2–b-TiO_2 particles were characterised by SEM. As shown in Fig. 2b, the N_2–b-TiO_2 particles are spherical with an average diameter size of 1–2 µm and a rough surface. The N_2–b-TiO_2 sample was further evaluated by EDS elemental mapping. As shown in Fig. 2c–f, the samples contain Ti, O, and N. The observed spatial distribution of Ti and O correspond to the TiO_2 spheres. Nitrogen is homogeneously dispersed over the entire sample area. The results further demonstrate that N had been successfully doped into the black TiO_2 spheres.

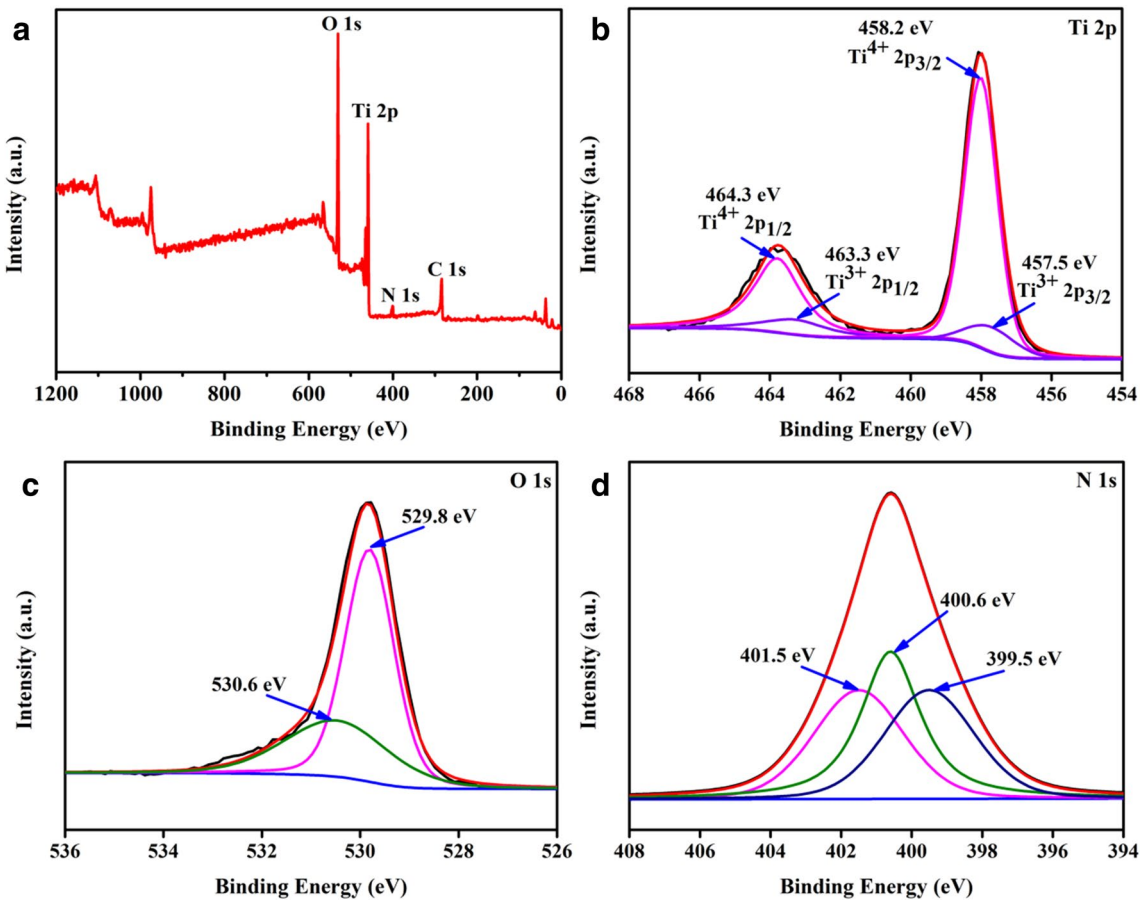

Fig. 4 **a** Survey XPS spectra, and **b** Ti 2p, **c** O 1s, and **d** N 1s spectra of N_2–b-TiO_2

As shown in Fig. 3a, the inner layer of the sample surrounded by blue line is crystalline, whereas the surface is disordered. The area surrounded by the blue line in Fig. 3a is enlarged in Fig. 3b, showing the lattice fringes with an inter-plane spacing of 0.35 nm. The corresponding fast Fourier transform (FFT) pattern (Inset) indicates that the lattice plane of N_2–b-TiO_2 is (101). Figure 3c is a low-magnification TEM image of the N_2–b-TiO_2 sample. The samples show a spherical morphology with a disordered surface. Based on earlier studies [29], this disordered outer layer may be caused by the introduction of Ti^{3+} and oxygen vacancies (O_V). At the same time, this disordered outer layer can provide electrons, and the crystal layer interface area acts as an electron transport channel. This structure has both a high carrier concentration and high electron mobility, which is beneficial to improving the photocatalytic performance. All these characteristics indicate that black TiO_2 spheres were prepared, and the process of nitrogen doping did not affect the morphology.

The chemical composition and surface chemical bonds of N_2–b-TiO_2 were investigated using XPS analysis. As shown in Fig. 4a, b-N-TiO_2 includes O, Ti, N, and C, which also proves the presence of nitrogen species. The carbon observed may be adventitious carbon contaminants or residual organic carbon from the XPS instrument or the external environment. As shown in Fig. 4b, peaks correspond to Ti^{4+} $2p_{1/2}$, Ti^{3+} $2p_{1/2}$, Ti^{4+} $2p_{3/2}$, and Ti^{3+} $2p_{3/2}$ were observed at binding energies of 464.3, 463.3, 458.2, and 457.5 eV, respectively [30]. As shown in Fig. 4c, the O 1s state of the sample shows two peaks at 530.6 and 529.8 eV, which represent two different O species in the sample. The binding energy of 530.6 eV corresponds to chemisorbed oxygen, dissociated oxygen, or OH groups on the surface. The shoulder peak observed at 529.8 eV corresponds to the O lattice of TiO_2 (Ti–O) [31]. For the N 1s peaks (Fig. 4d), the peak appeared at 399.5 eV after the substitution of N for O in the form of O–Ti–N bonding. The peak at 400.6 eV is attributed to the surface adsorption of N_2. The other peak at 401.5 eV can be assigned to the nitrogen species bound to various surface oxygen sites [32]. XPS analysis further confirmed that nitrogen had been successfully doped into the TiO_2 crystals.

The UV–Vis absorption spectra of the as-prepared samples are shown in Fig. 5a. Compared with the N_0–b-TiO_2 sample, the absorption of visible light by the nitrogen-doped black TiO_2 sample is obviously enhanced, which can be attributed to the doping by O_V, Ti^{3+}, and N, as well as the synergistic hydrogenation effect, which effectively reduces the bandgap of TiO_2 and increases the absorption of light [33]. As shown in Fig. 5b, the bandgap values of N_0–b-TiO_2, N_1–b-TiO_2, N_2–b-TiO_2, and N_3–b-TiO_2 are estimated to be 2.2, 2.0, 1.7, and 1.9 eV, respectively. Of the samples, N_2–b-TiO_2 has the narrowest band gap and the best photocatalytic ability, as discussed later.

The performance of the catalysts was studied via Cr(VI) and RhB degradation under visible light irradiation, as shown in Fig. 5b–f. After 150 min of visible-light irradiation, the photocatalytic efficiencies of N_0–b-TiO_2, N_1–b-TiO_2, N_2–b-TiO_2, and N_3–b-TiO_2 for potassium dichromate (10 mg/L) were 44.1, 65.6, 96.2, and 70.4% (Fig. 5b), respectively. Turning to the degradation of RhB,the N_0–b-TiO_2 catalyst showed negligible activity, and the degradation was 46.2% in 120 min. The rates of RhB degradation of N_1–b-TiO_2 and N_3–b-TiO_2 are 70.3% and 85.6%, respectively. Furthermore, N_2–b-TiO_2 achieved 99.5% degradation under visible light irradiation (Fig. 5c). These results are consistent with the UV–Vis results. The photocatalytic degradation of RhB is a pseudo-first-order reaction, and its kinetics can be expressed as $\ln(C_0/C) = k \times t$, where k is the photocatalytic reaction rate constant; the results are shown in Fig. 5d. The k values of N_0–b-TiO_2, N_1–b-TiO_2, N_2–b-TiO_2, and N_3–b-TiO_2 are 0.005, 0.009, 0.026, and 0.014 min^{-1}, respectively. The k value of N_2–b-TiO_2 is 5.2 times higher than that of N_0–b-TiO_2. The role of the active radicals in the N_2–b-TiO_2 sample was investigated using free radical trapping experiments, and the results are shown in Fig. 5e. Typically, hydroxyl radicals (•OH) and superoxide anions ($^{\bullet}O_2^-$) are the possible reactive species in the photocatalytic degradation. Tert-butyl alcohol (TBA), *p*-benzoquinone (BQ), and disodium ethylenediaminetetraacetic acid (Na_2-EDTA) were used as scavengers for the hydroxyl radicals (•OH), superoxide radicals ($^{\bullet}O_2^-$), and holes (h^+) [34]. When adding 5 mM BQ, the photocatalytic degradation efficiency of N_2–b-TiO_2 fell to 44.5%. Therefore, the efficiency of the photocatalytic degradation of RhB is obviously reduced after adding BQ, demonstrating that photogenerated $^{\bullet}O_2^-$ radicals were the dominant reactive species responsible for the high photocatalytic activity [35]. In addition, the visible light degradation stability of N_2–b-TiO_2 was examined by following the degradation of RhB during a five-cycle experiment. After each run, the catalyst was stirred in the dark for 30 min and reused in the next run. As shown in Fig. 5f, the degradation rates remained at 90.4% after five cycles. These results indicate that the use of N_2–b-TiO_2, which has a narrow bandgap and high photocatalytic reaction rate, results in excellent and stable photocatalytic activity.

Based on the above results, we proposed a possible photocatalytic mechanism for the N-doped black TiO_2 spheres. As shown in Fig. 6, the N doping results in a new impurity level above the valence band of TiO_2. Meanwhile, O_V and Ti^{3+} in the disordered outer layer form a new energy state under the conduction band of TiO_2 [36]. Moreover, the N-doped black TiO_2 spheres have a high surface area, which offers more active sites for photocatalytic reaction [37]. Under simulated visible light irradiation, the N-doped black TiO_2 spheres

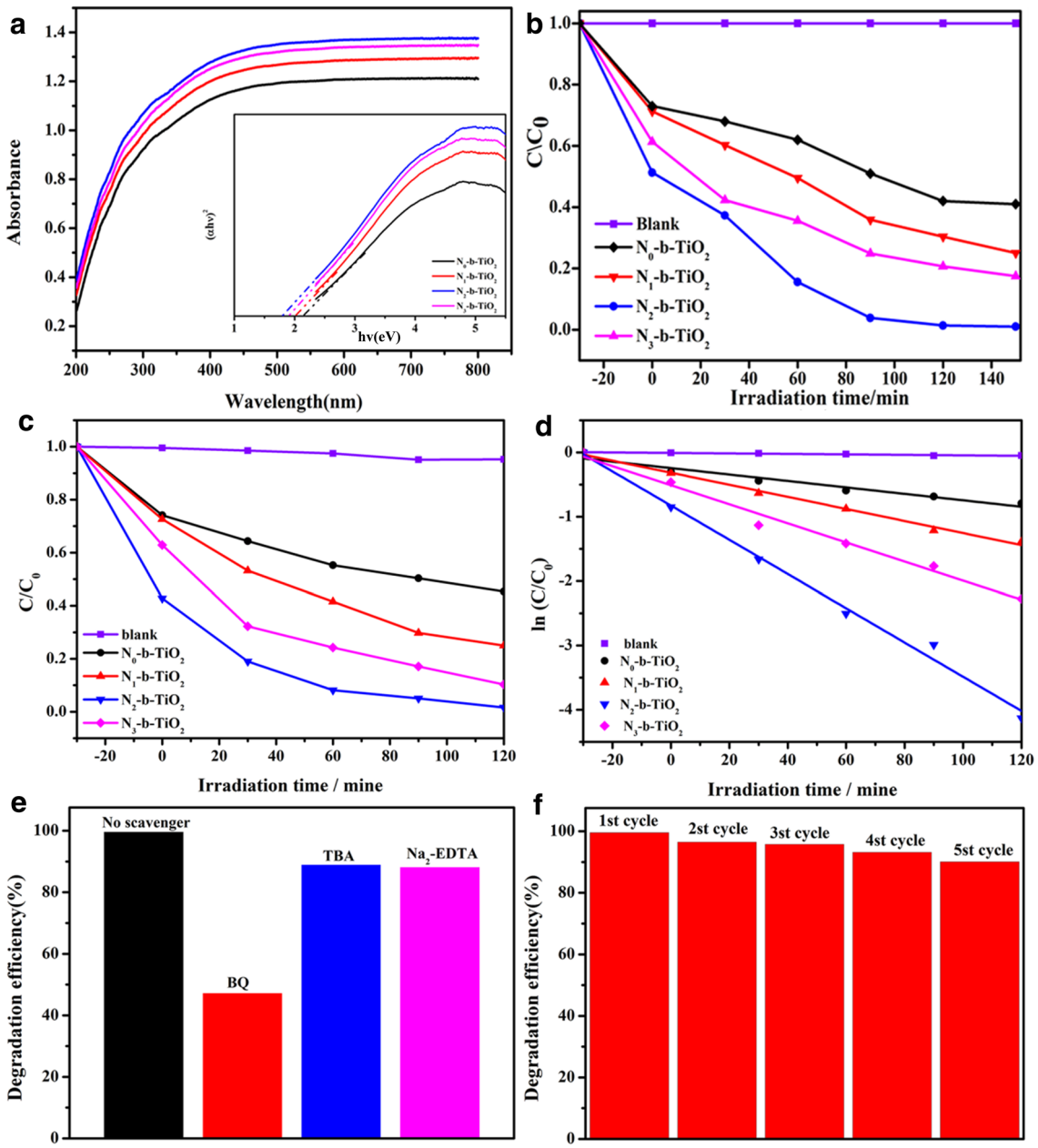

Fig. 5 **a** UV–Vis spectra and band gaps (inset) of N_0–b-TiO_2, N_1–b-TiO_2, N_2–b-TiO_2, and N_3–b-TiO_2. Photocatalytic process of potassium dichromate (**b**) and RhB (**c**) for different catalysts under visible light irradiation. **d** Changes in the ln(C/C_0) versus visible light irradiation time for different catalysts. **e** Trapping test of photogenerated holes and radicals with N_2–b-TiO_2. (f) The degradation cycles of RhB using N_2–b-TiO_2 as photocatalysts after visible light irradiation for 2 h

were excited to produce photoelectron–hole pairs. The photogenerated electrons are excited from the valence band (VB) of the N-doped black TiO_2 spheres to the conduction band (CB), and holes are left in the valence band. At the same time, a new energy state with a high concentration of Ti^{3+} and oxygen vacancies is formed below the conduction band of TiO_2, suppressing the recombination of electron–hole pairs. In the photocatalytic process, photogenerated electrons are involved in the redox reaction of the Cr(VI)-to-Cr(III) conversion and react with oxygen (O_2) to form superoxide radicals ($\bullet O_2^-$). Meanwhile, the photogenerated holes react with water (H_2O) or hydroxide ions (OH^-) adsorbed on the surface of the catalyst to generate hydroxyl radicals

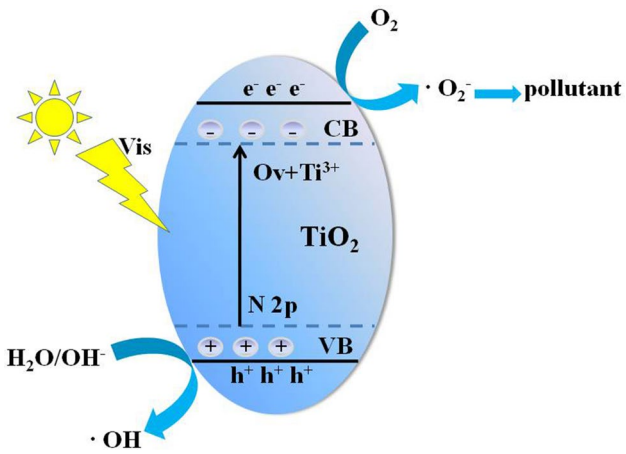

Fig. 6 Schematic photocatalytic mechanism of N_2–b-TiO_2

(•OH). Finally, $•O_2^-$ radicals with strong reducing power are used to decompose pollutants. This is consistent with the experimental results obtained with the sacrificial agents, which indicate that $•O_2^-$ radicals are the main active groups responsible for maintaining the high photocatalytic activity of the N-doped black TiO_2 spheres. Therefore, the excellent photocatalytic performance of N-doped black TiO_2 spheres can be attributed to three factors: (1) Nitrogen doping generates new impurity levels above the valence band of TiO_2, which absorbs visible light in sunlight effectively; (2) O_V and Ti^{3+} in the disordered outer layer form a new energy state under the conduction band of TiO_2, which inhibits the electron–hole pair recombination; and (3) the large specific surface area of the spheres provides more active sites, which makes contact between the reactants and the catalysts easier and improves the photocatalytic performance.

4 Conclusion

In summary, N-doped black TiO_2 spheres were successfully synthesised by a simple solvothermal method. The morphological and structural analyses confirmed that N species had been incorporated into the black TiO_2 spheres. The N doping results in a new impurity level above the valence band of TiO_2, and O_V, Ti^{3+} in the disordered outer layer form a new energy state under the conduction band of TiO_2, which can effectively enhance the absorption of visible light and inhibits electron–hole pair recombination. Moreover, the spherical structure provides many active sites. Therefore, the efficiency of the degradation of Cr(VI) and RhB by the N_2–b-TiO_2 spheres was as high as 96.2% and 99.5%, repectively. Trapping of the photogenerated holes and radicals of N_2–b-TiO_2 confirmed that superoxide radicals ($•O_2^-$) played a crucial role in the degradation of the organic pollutant. This work demonstrates a method for optimizing composite semiconductor catalysts from morphology and band structure, providing a good reference for comprehensive improvement of semiconductor photocatalysis.

Acknowledgements This work was supported by the National Natural Science Foundation of China (Grant Nos.11264037, 51602273, 61464010, and 61604126), Wuhan University of Technology (2018-KF-14), and Natural Science Foundation of Xinjiang (2017D01C055).

Compliance with ethical standards

Conflict of interest The authors declare that they have no confict of interest.

References

1. Wang H, Zhang L, Chen Z et al (2014) Semiconductor heterojunction photocatalysts: design, construction, and photocatalytic performances. Chem Soc Rev 43:5234–5244
2. Zhou W, Li W, Wang et al (2014) Ordered mesoporous black TiO_2 as highly efficient hydrogen evolution photocatalyst. J Am Chem Soc 136:9280–9283
3. Sun B, Zhou W, Li H et al (2018) Synthesis of particulate hierarchical tandem heterojunctions toward optimized photocatalytic hydrogen production. Adv Mater 30:1804282
4. Elghniji K, Ksibi M, Elaloui E et al (2012) Sol–gel reverse micelle preparation and characterization of N-doped TiO_2: efficient photocatalytic degradation of methylene blue in water under visible light. J Ind Eng Chem 18:178–182
5. Liu H, Wu R, Tian L et al (2018) Synergetic photocatalytic effect between 1T@2H-MoS_2 and plasmon resonance induced by Ag quantum dots. Nanotechnology 29:285402
6. Zhou W, Fu H et al (2018) Defect-mediated electron–hole separation in semiconductor photocatalysis. Inorg Chem Front 5:1240
7. Zhang Y, Jiang L, Huang Y et al (2015) Titanate and titania nanostructured materials for environmental and energy applications: a review. RSC Adv 5:79479–79510
8. Ge M, Cao C, Huang J et al (2016) A review of one-dimensional TiO_2 nanostructured materials for environmental and energy applications. J Mater Chem A 4:6772–6801
9. Fan M, Wu R, Liu Y et al (2018) Synthesis of metal-phase-assisted 1T@2H-MoS_2 nanosheet-coated black TiO_2 spheres with visible light photocatalytic activities. J Mater Sci 53:10302–10312
10. Chen Y, Liu K et al (2016) Preparation and characterization of nitrogen-doped TiO_2/diatomite integrated photocatalytic pellet for the adsorption-degradation of tetracycline hydrochloride using visible light. Chem Eng J 302:682–696
11. Morikawa T, Asahi R, Ohwaki T et al (2001) Band-gap narrowing of titanium dioxide by nitrogen doping. Jpn J Appl Phys 40:L561–L563
12. Asahi R, Morikawa T, Ohwaki T et al (2001) Visible-light photocatalysis in nitrogen-doped titanium oxides. Science 293:269–271
13. Xiaobo C, Lei L, Yu PY et al (2011) Synthesis and characterization of composite visible light active photocatalysts

MoS_2–g-C_3N_4 with enhanced hydrogen evolution activity. Science 331:746–750
14. Lu H, Zhao B, Pan R et al (2013) Safe and facile hydrogenation of commercial Degussa P25 at room temperature with enhanced photocatalytic activity. Rsc Adv 4:1128–1132
15. Lin T, Yang C, Wang Z et al (2014) Effective nonmetal incorporation in black titania with enhanced solar energy utilization. Energy Environ Sci 7:967
16. Xin L, Shanmin G, Hui X et al (2013) Ti^{3+} self-doped TiO_2 photoelectrodes for photoelectrochemical water splitting and photoelectrocatalytic pollutant degradation. Nanoscale 5:1870–1875
17. Fang Y, Wang J, Li J et al (2016) Preparation and application of black hollow carbon-doped titania composite spheres for electrophoretic displays. J Mater Sci Mater Electron 27:6115–6121
18. Panomsuwan G, Watthanaphanit A, Ishizaki T et al (2015) Water-plasma-assisted synthesis of black titania spheres with efficient visible-light photocatalytic activity. Phys Chem Chem Phys 17:13794–13799
19. Wei S, Wu R, Xu X et al (2016) Synthesis of Large—area MoS_2 atomic layers with chemical vapor deposition. Chem Eng J 299:120–125
20. Hu W, Zhou W, Zhang K et al (2016) Facile strategy for controllable synthesis of stable mesoporous black TiO_2 hollow spheres with efficient solar-driven photocatalytic hydrogen evolution. J Mater Chem A 4:7495–7502
21. Cao Y, Xing Z, Shen Y et al (2017) Mesoporous black Ti^{3+}/N-TiO_2 spheres for efficient visible-light-driven photocatalytic performance. Chem Eng J 325:199–207
22. Idris A, Hassan N, Rashid R et al (2011) Kinetic and regeneration studies of photocatalytic magnetic separable beads for chromium (VI) reduction under sunlight. Water Res 186:629–635
23. Huang L, Fu W, Fu X et al (2017) Facile and large-scale preparation of N doped TiO_2 photocatalyst with high visible light photocatalytic activity. Mater Lett 209:585–588
24. Yun Z, Liu Y, Li J et al (2017) Synthesis and characterization of visible-light-active mesoporous titania by doping Ni and N. J Mater Sci Mater Electron 28:18164–18172
25. Wang Y, Feng C, Zhang M et al (2011) Visible light active N-doped TiO_2 prepared from different precursors: origin of the visible light absorption and photoactivity. Appl Catal B 104:268–274
26. Xiao L, Liu P, Yu M et al (2015) Preparation of homogeneous nitrogen-doped mesoporous TiO_2 spheres with enhanced visible-light photocatalysis. Applied Catalysis B. Appl Catal B Environ 164:352–359
27. Nakamura R, Tanaka T, Nakato Y et al (2004) Mechanism for visible light responses in anodic photocurrents at N-doped TiO_2 film electrodes. J Phys Chem B 108:10617–10620
28. Zhang X, Chen Z (2015) Enhanced photoelectrochemical performance of the hierarchical micro/nano-structured TiO_2 mesoporous spheres with oxygen vacancies via hydrogenation. RSC Adv 5:9482–9488
29. Lü X, Chen A, Luo Y et al (2016) Conducting interface in oxide homojunction: understanding of superior properties in black TiO_2. Nano Lett 16:5751–5755
30. Hoang S, Guo S, Hahn NT et al (2012) Visible light driven photoelectrochemical water oxidation on nitrogen-modified TiO_2 nanowires. Nano Lett 12:26–32
31. Jaiswal R, Patel N, Kothari DC et al (2012) Improved visible light photocatalytic activity of TiO_2 co-doped with vanadium and nitrogen. Appl Catal B Environ 126:47–54
32. Li H, Hao Y, Lu H et al (2015) A systematic study on visible-light N-doped TiO_2 photocatalyst obtained from ethylenediamine by sol–gel method. Appl Surf Sci 344:112–118
33. Zhang K, Zhou W, Chi L et al (2016) Black N/H–TiO_2 nanoplates with a flower—like hierarchical architecture for photocatalytic hydrogen evolution. Chemsuschem 9:2841–2848
34. Weiyin G, Minqiang W, Chenxin R et al (2015) Facile one-pot synthesis of MoS_2 quantum dots–graphene–TiO_2 composites for highly enhanced photocatalytic properties. Chem Commun 51:1709
35. Nimbalkar DB, Lo H-H, Ramacharyulu PVRK et al (2016) Improved photocatalytic activity of RGO/MoS_2 nanosheets decorated on TiO_2 nanoparticles. RSC Adv 6:31661–31667
36. Pei Z, Ding L, Lin H et al (2013) Facile synthesis of defect-mediated TiO_{2-x} with enhanced visible light photocatalytic activity. J Mater Chem A 1:10099–10102
37. Yang HM, Park SJ (2016) Influence of mesopore distribution on photocatalytic behaviors of anatase TiO_2 spherical nanostructures. J Ind Eng Chem 41:33–39